PERGAMON

Journal of Structural Geology 22 (2000) 1541–1557

JOURNAL OF STRUCTURAL GEOLOGY

www.elsevier.nl/locate/jstrugeo

Texture analysis of a muscovite-bearing quartzite: a comparison of some currently used techniques

Klaus Ullemeyer[a,*], Günter Braun[b], Michael Dahms[c], Jörn H. Kruhl[d], Niels Ø. Olesen[e], Siegfried Siegesmund[a]

[a]*Institut für Geologie und Dynamik der Lithosphäre, Goldschmidtstr. 3, 37077 Göttingen, Germany*
[b]*Institut für Geowissenschaften, Olshausenstr. 40-60, 24118 Kiel, Germany*
[c]*GKSS Forschungszentrum, Max-Planckstr. 12, 21502 Geesthacht, Germany*
[d]*Institut für Geologie, Geotechnik und Baubetrieb, Arcisstr. 21, 80290 München, Germany*
[e]*Department of Earth Sciences, C.F. Møllers Alle, 8000 Åarhus C, Denmark*

Received 14 December 1999; accepted 28 June 2000

Abstract

Four well-established techniques were applied to determine the mineral textures of a muscovite-bearing quartzite: (1) directional measurements on an optical U-stage; (2) X-ray; (3) neutron; and (4) electron diffraction (EBSD). Techniques (1) and (4) are of the 'single grain' type and techniques (2) and (3) of the 'statistical' or 'volume' type. Experimental pole density diagrams were compared by means of the construction of pole figure differences ('difference pole figures'), which led to the observation that EBSD- and U-stage derived pole figures agree well, even in detail. In contrast, pole figures derived from X-ray and neutron diffraction are clearly different from pole figures derived from the single grain techniques, visible as pronounced preferred orientation in the difference pole figures. Specific properties of the applied techniques may be responsible for the observed differences, such as (1) missing proportionality to the grain volume in the single grain methods, (2) the accessible sample volume, (3) erroneous data correction, or (4) statistical errors. Also the method of data treatment, which is basically different for the single grain and statistical methods, should be considered when pole figures are evaluated. Apart from purely economical constraints and availibility of equipment, the decision on the most suitable method for a texture determination should be based on the scientific goals and specific properties of particular techniques. Texture measurements of the statistical type are well suited for determination of bulk textures of rocks (e.g. as required for the calculation of anisotropic physical properties of rocks), whereas single grain measurements are advantageous for the investigation of local textures and texture forming mechanisms.

1. Introduction

The lattice preferred orientation, or texture, of rock forming minerals is related to the deformation history of the rock and to its physical properties. Texture investigations are routinely performed with the following three main goals.

1. Deconvolution of the deformation history of rocks on the basis of the symmetry of the mineral textures, which commonly reflects the symmetry of deformation, has been the subject of many studies, with a focus on quartz (e.g. Bouchez and Pecher, 1981; Schmid and Casey, 1986; Law, 1990), carbonates (e.g. Erskine et al., 1993; Leiss, 1996), phyllosilicates (e.g. Oertel, 1985; O'Brien et al., 1987), and olivine (e.g. Wedel et al., 1992; Van der Wal and Vissers, 1996).
2. The modelling of physical anisotropies of rocks. Since all minerals are anisotropic with regard to physical properties such as the elastic, thermal and magnetic properties, the anisotropy of bulk rock also depends upon the texture (refer to Siegesmund, 1996 for a review). For example, the elastic properties of rocks are related to the rock fabric and therefore can support the geological interpretation of geophysical anisotropies in the earth's crust (e.g. Rabbel et al., 1998) and upper mantle (Weiss et al., 1999). Texture determinations can also be of importance to the Society: the mechanical weathering of marble building stones is partly controlled by the anisotropic intrinsic rock properties (e.g. Siegesmund et al., 2000).
3. The understanding of the texture-forming processes in rocks. Lattice preferred orientations result from various

* Corresponding author. Fax: +49-551-399700.
E-mail address: kulleme@gwdg.de (K. Ullemeyer).

0191-8141/00/$ - see front matter
PII: S0191-8141(00)00103-6

Table 1
Overview of the applied methods and equipment for texture measurements. The references either give an introduction to the measuring principle, to the applied instrument or to improvements of the basal technique; the last column indicates the resulting data type

Method	Applied equipment	References	Data type
Electron backscattering diffraction (EBSD)	SEM with Nordif EBSD system	Joy et al., 1982; Lloyd, 1985; Schmidt and Olesen, 1989	Directions of any lattice plane normal, mostly with sign
Optical microscopy	Leitz U-stage on a Leitz polarization microscope	Reinhard, 1931; Panozzo-Heilbronner and Pauli, 1993	Quartz: *c*-axis orientation Muscovite: orientation of optical indicatrix axes $n_\alpha, n_\beta, n_\gamma$
X-ray diffraction	Backreflection texture diffractometer	Schulz, 1949; Braun, 1994	Pole density distribution of one or more Bragg lines
Time-of-flight neutron diffraction	Multidetector texture diffractometer	Schäfer et al., 1995; Walther et al., 1995; Ullemeyer et al., 1998	Pole density distribution of one or more Bragg lines

physical processes (e.g. dislocation slip, diffusion of material) and external parameters, such as volume fraction, composition and distribution of phases, temperature, pressure and the type of stress and strain (Skrotzki, 1994). Such processes are input parameters for texture simulations which seek to reproduce naturally observed textures.

Lattice preferred orientations can be measured by determination of the orientation of selected lattice directions, or the complete orientation of individual crystals in the sample (*single grain measurements*). Optical microscopy and electron diffraction (backscattered or channeling patterns) are applied for that purpose. Alternatively, preferred orientation measurements can be carried out in a statistical diffraction experiment determining pole density distributions or pole figures (integrating *volume texture measurements*). X-rays and neutrons are applied most commonly, synchrotron radiation to a minor extend. All these fundamental methods possess specific restrictions and lead to more or less complete textural information. In addition, different procedures of data treatment are required to obtain the most comprehensive texture information from an experimental data set. This paper gives an overview of these methods of texture determination. The fundamental physical principles are briefly outlined, and references are given to the experimental techniques which have been developed in the last decades. Four techniques frequently applied in geosciences: optical U-stage; electron backscatter diffraction (EBSD) technique; X-ray backreflection texture goniometry; time-of-flight neutron diffraction, were applied to determine the texture of a two-phase muscovite–quartzite (Table 1), and advantages and disadvantages of these methods of texture determination are discussed based on our data. Although the paper focuses on the comparison of experimental pole figures, some aspects related to the mathematical methods of texture analysis are addressed as well.

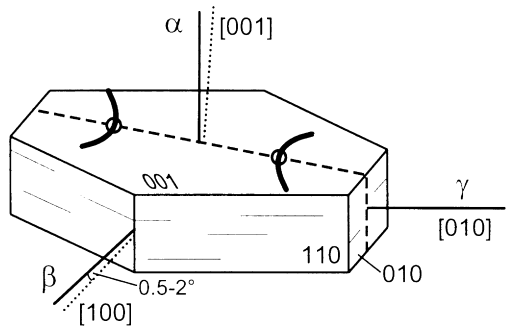

Fig. 1. Muscovite crystal with optical and crystallographic orientations (Tröger, 1971).

2. Experimental methods of texture analysis

From the subdivision of experimental methods into 'single grain' methods and 'volume' or 'statistical' methods, two principle properties are obvious. The measuring of single crystals allows the determination of the location parameters of each grain in addition to the orientation parameters. Hence, grain–grain relationships like orientation differences are determinable, and the distribution in the acquisition surface of selected lattice directions ('Achsenverteilungsanalyse', Sander 1934) or even complete orientations (Leiss et al., 1994) can be investigated. However, the measurements are not related to the grain volume except for the special case of equant grain size. In a 'statistical' diffraction experiment the proportionality to the scattering volume fraction is given, but it is impossible to locate the orientation of a single grain. Apart from these joint characteristics, specific properties control the experimental possibilities and these are summarized below.

2.1. Universal stage measurements (optical methods)

Optical orientation measurements are based on the anisotropic optical properties of the minerals. The properties depend upon crystal symmetry and can be described by the optical indicatrix with its axes n_α, n_β, n_γ, n: refractive index (Wenk, 1985). Cubic minerals are isotropic, therefore orientation measurements are not possible. In the case of trigonal, hexagonal and tetragonal crystal symmetry one optical axis (direction of isotropy) exists. It corresponds to

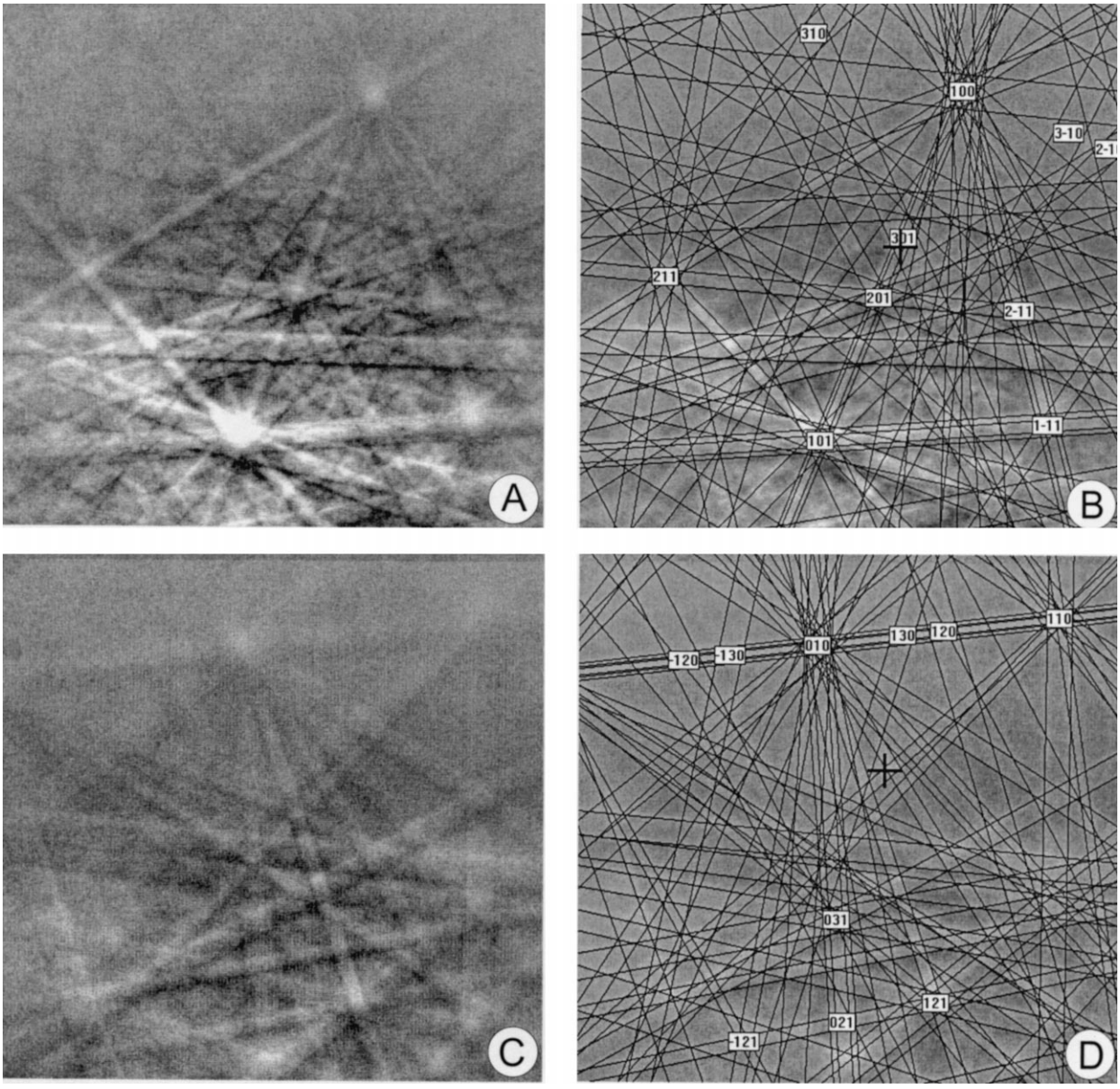

Fig. 2. (A) Live, but processed, EBSD image of quartz; 25 kV. (B) Image in (A) is indexed with application of the software package CHANNEL©. (C) Live, but processed, EBSD image of muscovite; 25 kV. (D) Image in (C) is indexed with application of the software package CHANNEL©.

the crystallographic *c*-axis which represents the only measurable lattice direction. Orthorhombic, monoclinic and triclinic minerals have two optical axes with different orientation relationships to the crystal lattice: in orthorhombic minerals, the indicatrix axes parallel the crystallographic axes; in monoclinic minerals like muscovite, one indicatrix axis parallels the crystallographic [010] axis (Fig. 1). Triclinic minerals show a variable relationship between orientation of the indicatrix and the crystallographic axes. In all these cases there are variations dependending upon the mineralogical composition. In fact, in order to determine the complete orientation of low-symmetry minerals the orientation of specific lattice planes must be determined in addition to the indicatrix axes. Based on these data the complete orientation may be established by geometrical constructions (e.g. Burri et al., 1967: plagioclase). However, all these operations are very time-consuming but can be accelerated considerably by means of computer codes (Kruhl, 1987; Benn and Mainprice, 1989; Cumbest, 1990). Photometric methods (Price, 1973; Panozzo-Heilbronner and Pauli, 1993) apply image processing to determine orientation distributions automatically with minor manual effort. They are solely applicable to uniaxial minerals such as quartz. A major restriction for optical orientation measurements is the grain size, since very small grains (<50 μm) cannot be measured by an optical microscope.

2.2. Electron diffraction

When an electron beam hits a crystalline target electrons penetrate the surface. A fraction of these electrons are backscattered (i.e. reflected at a high angle) due to interactions with the nucleus of the atoms. Some of these electrons succeed in escaping to the surface of the target with energies close to the original energy. During this escape the organisation of the atoms of the crystalline target is reflected in the spatial variation in the intensity of the backscattered electrons, i.e. the electrons are diffracted by the lattice following Bragg's law ($2d \sin \Theta = \lambda$).

The variation in intensity is best explained considering the electrons as waves (e.g. Joy et al., 1982). The Bloch wave theory predicts that electrons travelling parallel to lattice planes will have a high intensity, while electrons travelling at an angle to lattice planes which is greater than the relevant Bragg angle (Θ) have a low intensity. A dramatic change in intensity takes place across the Bragg angle itself. Consequently, the spatial variation in the intensity of the backscattered electrons is such that the intensity is high in a direction parallel to a lattice plane $\pm$ the relevant Bragg angle (Θ).

The EBSD technique takes advantage of this fact by intercepting the cloud of backscattered electrons with a phosphor screen, where light bands (with a width corresponding to 2Θ) on a dark background (Fig. 2A, C) reflect the three-dimensional orientation of lattice planes in the crystalline target. A plane polished specimen is mounted in a scanning electron microscope and tilted such that the angle between the beam and the normal to the specimen surface is 70°. A stationary beam hits the surface and backscattered electrons are diffracted by any crystal lattice hit by this beam. A live diffraction pattern with a solid angle of approximately 70° is created on the phosphor screen, which is placed in a vertical position close to the specimen. The phosphor screen is viewed from behind by a CCD camera, and after image processing, such as background subtraction, the live diffraction pattern may be analysed and indexed (Fig. 2B, D). The quality of the image of the diffraction pattern depends critically upon factors such as the quality of the polish of the acquisition surface, but also of the mineral composition and lattice structure. Diffraction images of muscovite (Fig. 2C) are clearly of a lower quality (low contrast and diffuse band edges) than diffraction images of quartz (Fig. 2A), acquired from neighbouring grains.

The microstructure of the tilted specimen is viewed as an absorbed current image, which permits observation of diffraction patterns from known positions on the acquisition surface. The spatial resolution is approximately 1 μm (Hjelen and Nes, 1990). The uncertainty of absolute crystal lattice orientation determinations are estimated to be about 3° (Hjelen et al., 1993), where the uncertainty is likely to be $>3°$ in the case of muscovite and $<3°$ in the case of quartz, due to the variations in image quality.

In principle, by application of the EBSD (and the related electron channeling pattern (ECP)) technique, the lattice orientation of any crystal which is hit by the beam can be determined to the level of Laue Group symmetry (e.g. Schmidt and Olesen, 1989, Olesen and Schmidt, 1990). This means that measurements of quartz permit construction of fabric diagrams of all crystallographic planes and directions. All directions are known *with sign*, with the important exception of the directions lying in the $\{11\bar{2}0\}$ planes (the FLMPs of Olesen and Schmidt, 1990), which include the *c*, *r* and *z* directions. Measurements of muscovite permit construction of fabric diagrams of all crystallographic planes and directions as well, and again the directions are known *with sign* except for those lying in (010), which is the plane of symmetry.

2.3. X-ray diffraction

X-ray diffraction is based on the interaction of electromagnetic radiation with the hull electrons of the atoms. It may be treated as mirror reflection on virtual lattice planes, which connect the structurally defined atom positions in a crystal lattice (e.g. Azaroff, 1968). Bragg's law relates the wavelength λ to the lattice spacing d and the scattering angle Θ. For application to pole figure measurements, the angle Θ is set to the correct value of the desired Bragg reflection (*hkl*) and kept constant. Subsequently, the spatial orientation of the sample is systematically changed in a two-circle goniometer and the intensity I_r of the reflected beam is measured by an X-ray counter tube at each sample position (α, β). Since the reflected intensity is proportional to the scattering volume portion $\Delta V(\alpha, \beta)$, it represents a measure for the degree of preferred orientation.

The two standard methods for pole figure measurements have been known since the beginning of diffraction measurement. In the backreflection technique, the scattered beam is observed at the incident side of the sample (Schulz, 1949). The sample must be impermeable for X-rays to avoid intensity loss. In transmission mode, the beam passes through the sample (Decker et al., 1948), which in contrast to the backreflection method must be thin enough (in the magnitude of 50 μm for most minerals). Each method requires specific corrections of progressive intensity loss in the course of the experiment. Since the path through the sample extends with increasing tilt angle, an absorption correction is obligatory for the transmission technique. A defocusing correction is required for the backreflection technique because the diffraction peak broadens due to changing focusing conditions with increasing tilt angle (Chernock and Beck, 1952; Von Gehlen, 1960; Ortiz and Hermida, 1981). The worsening of counting statistics limits the measurable pole angle range. This range is usually $>60°$ (transmission mode) and $<70°$ (backreflection mode), respectively. The correction coefficients may be deduced theoretically from the experiment geometry or from a random sample measurement of the material investigated.

At least three mutually perpendicular samples measured

Table 2
Penetration depth $d_{0.5}$ for X-rays and neutrons of some rock-forming minerals; the parameter $d_{0.5}$ characterizes the sample thickness, at which the incoming intensity is reduced to the half (data from Brokmeier, 1994)

Mineral	$d_{0.5}^{\text{X-rays}}$, μm	$d_{0.5}^{\text{neutrons}}$, μm	$d_{0.5}^{\text{neutrons}}/d_{0.5}^{\text{X-rays}}$
Quartz	75.9	24 300	320
Albite	81.0	24 800	306
Calcite	36.0	19 800	550
Biotite	18.1	6410	354
Muscovite	57.9	7940	137
Halite	42.0	8140	194
Amphibole	25.0	9690	388

either in backreflection or transmission mode are required to obtain complete pole figures. Since in backreflection mode the inner part of the pole figure is measured and in transmission mode the outer one, the combination of a backreflection and a transmission measurement from a single section also leads to complete pole figures. In that case, different sample preparation techniques and different methods of intensity correction are required to ensure the proper adaptation of the two pole figure ranges.

More advanced measuring techniques apply position sensitive detectors in Θ which allow the recording of short diffraction patterns, usually some degrees (2Θ). This has two advantages: (i) partly overlapping Bragg reflections can be mathematically separated by means of peak profile analysis; and (ii) the peak broadening due to defocusing is recorded, hence, the measurable pole figure range can be extended up to 85° and often completed by means of an interpolation procedure. The measurements on the considered specimen were carried out in a different way: a short 2Θ scan within a range of 3.8° was carried out at each sample position. Separate integration of the intensities to the left and to the right of the center line of the diffraction peak (which is assumed to be symmetrical) leads to two intensity values. Only the one which is free from overlapping is used as a measure for the pole density (Braun, 1994). By this method, pole figure measurements can be carried out on slightly overlapping Bragg reflections with sufficient accuracy, although peak separation by curve fit procedures is not applied.

2.4. Neutron diffraction

Thermal neutrons with a kinetic energy of 5–500 MeV are characterized by wavelengths λ in the magnitude of the atomic diameter. Therefore, they are well suited for a diffraction experiment according to Bragg's law, although the interaction of neutrons with matter is quite different compared with X-rays. Neutron scattering is mainly controlled by the interaction of the neutron with the atomic nucleus and may be quantified by the scattering length b. Since the nucleus is very small with respect to the wavelength λ of the radiation, the scattering length b does not depend on the scattering angle Θ. In the case of X-rays b decreases with increasing Θ. Hence, also Bragg reflections with high index may be measured with neutrons. Furthermore, there is no interdependence between the scattering length b and the atomic number Z (in the case of X-rays it increases with increasing atomic number). Therefore, the scattered intensity is not dominated by heavy elements, which might be of importance for some minerals. For more details on the fundamentals of neutron scattering refer to Bacon (1975).

The most significant property of neutrons is their low absorption in matter. Compared to X-rays, the penetration depth of neutrons is 10^2 to 10^4 times larger for most minerals (see Table 2) and therefore much larger sample volumes (several cubic centimeters) can be investigated. This offers additional possibilities for texture analysis: coarse-grained samples can be investigated, as well as samples which are inhomogeneous with respect to mineral distribution and texture (Siegesmund et al., 1994). This is especially important for the calculation of rock physical anisotropies, which are controlled by the bulk rock volume. If the sample shape approximates to a sphere, no absorption correction is required; cubes, cylinders and also irregular sample shapes are all suitable for neutron texture measurements. In contrast to X-ray measurements which require polished sample surfaces or thin films, no special sample preparation techniques are necessary and complete pole figures can be measured with only one sample. As a disadvantage, the relatively low intensity of the neutron beam compared with the intensity of an X-ray beam must be mentioned. This results in a longer measuring time to obtain complete pole figures. As a compensation, position-sensitive or multidetector systems are installed at many neutron facilities (e.g. Schäfer et al., 1995) and/or all wavelengths are used for the experiment (time-of-flight diffraction; Ullemeyer et al., 1998). This allows the recording of more or less complete diffraction patterns, i.e. several pole figures can be measured simultaneously and peak profile analyses to deconvolute partly overlapping Bragg reflections are applicable (e.g. Wenk et al., 1986).

3. Mathematical methods of texture data analysis

The data sets obtained from 'single grain' and 'volume' diffraction measurements are of a different nature. In the first case, either the complete spatial orientations or the spatial orientations of one (or more) lattice directions of a finite number of mineral grains are known. In the second case, spatial pole density variations are obtained. Both require different methods of data treatment and offer different possibilities.

Knowledge of the complete orientation of a crystal allows calculation of all desired lattice directions on the basis of the lattice constants. The lattice directions can be plotted directly in a stereonet, although pole density distributions are usually calculated from the directional data. Widely

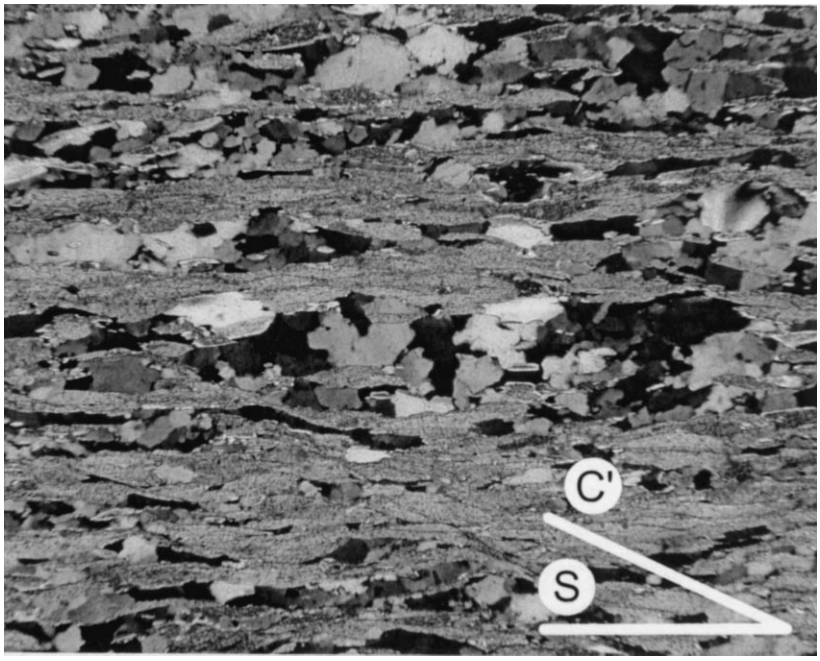

Fig. 3. Optical micrograph of the sample in the section perpendicular to S and parallel to L. Crossed polarizers. The orientations of schistosity (S) and widely spaced shear bands (C′) are indicated. The length of the schistosity bar is 1 mm.

used in geology is the counting of all measured directions up to a maximum angular distance from the orientation of a 'counting grid' point, without weighting the direction based upon the angular distance (Braun, 1969). Alternatively, weight functions can be applied, e.g. a Gauss distribution or harmonics (Adam, 1989: cosine between measured direction and counting grid point). Although the calculated density data are usually normalized to get multiples of a random distribution, the quantities obtained from these methods are usually different. In addition to the properties of the applied function, the quantities depend upon the selected maximal distance between direction and counting grid point, or the critical parameter of the weight function (e.g. the half width of the Gaussian), or the power applied to the cosine. Varying these parameters corresponds to a more or less pronounced smoothing of the pole density distribution, but there is no obvious criterion which leads to the 'true' one. This fact also hampers the comparison of pole figures obtained from 'single grain' and 'statistical' diffraction measurements.

The data set obtained from a 'statistical' diffraction experiment consists of pole density distributions (pole figures) of one or more lattice planes. To obtain the complete mineral texture, the three-dimensional orientation distribution function $f(g)$, g: orientation; (ODF; Bunge, 1982) must be calculated from a number of input pole figures, which are two-dimensional projections of the ODF. Subsequently, all desired lattice directions can be calculated from the ODF, such as the quartz (001) pole figure which is important for texture interpretations but cannot be measured directly. Calculation of the ODF requires some mathematical effort. The precision depends upon the number and quality of the measured pole figures and on the crystal symmetry of the mineral concerned. As an example, a single incomplete (111) pole figure is sufficient for minerals with cubic symmetry. The solution of the ODF equation is further complicated by the fact that anti-parallel directions cannot be distinguished in a diffraction experiment (Friedel's law). Thus, a range of possible solutions exists. Only additional assumptions and boundary conditions such as the positivity condition (Dahms and Bunge, 1988) can lead to a unique ODF.

The applied pole figure inversion methods can be separated into *continuous* and *discrete* methods. In the continuous methods, the ODF is developed into a finite series of known continuous functions. In the classical harmonic method, these functions are generalized spherical harmonics (Dahms and Bunge, 1989). In the more recent component method, the texture is described by a finite number of single crystal orientations. Three-dimensional Gauss distributions are used to describe the intensity decrease with increasing angular distance from the ideal orientation of the single crystal (Helming and Eschner 1990, Eschner 1993). The discrete methods: (1) the vector method (Schaeben et al., 1985); (2) WIMV (Matthies and Vinel, 1982); and (3) MENTEX (Schaeben and Siemes, 1996) directly result in values of the ODF at previously defined points in Euler space. The major advantage of WIMV and MENTEX is that the positivity condition is included in their basic algorithm. A certain disadvantage is that neighbouring points in Euler space are not coupled, such that the result of the pole figure inversion often has to be smoothed in order to make it readable. Similar effects are observed using the geometrical method of crystal-dicing (Braun 1994). The smoothing is

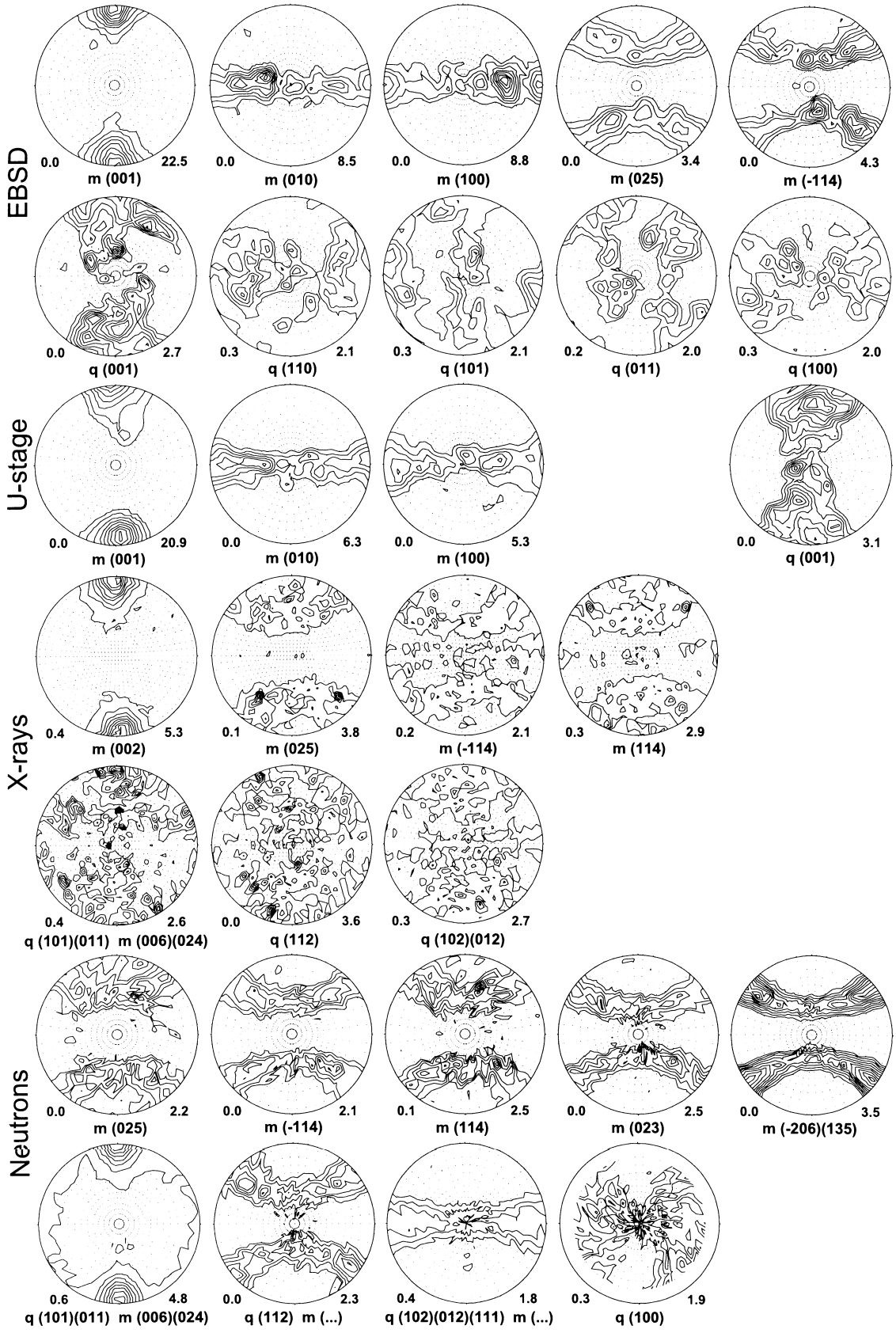

Fig. 4. Selected experimental pole figures obtained with different experimental techniques. Intensities are given as multiples of a random distribution, dots indicate regions with intensities <1.0 [m.r.d.]. Minimum and maximum intensity are indicated at the bottom of each plot. For details about the calculation of density distributions from directional measurements (U-stage and EBSD data), refer to text.

done when transforming the weights of each set of (*hkl*) faces (the result of crystal-dicing) into a modelled set of elementary reflections using a range of influence around each (*hkl*) position and randomly generated coordinates.

It should be expected that all existing methods lead to comparable results assuming that pole figures are measured with good quality. In the case of weak textures and input pole figures with a high level of statistical and/or systematic errors, different methods lead to quantitatively different ODFs, although qualitative features, e.g. the position of major texture components, will always be resolved in the same way. In this case, the positivity method has the tendency to produce very smooth ODFs, whereas the component method and crystal dicing result in textures with enhanced maxima. The question arises whether the method of ODF calculation influences the interpretation of the texture.

4. Sample description

A specimen of a fine-grained muscovite quartzite was collected from a rock sequence of the Matreier zone which is situated in the western Tauern window, Austrian Alps (Raith et al., 1977). It contains $\approx 50\%$ muscovite, $\approx 49\%$ quartz, and $\approx 1\%$ other minerals. The quartzite exhibits a well-developed compositional layering (<1 mm) defined by quartz- and muscovite-rich layers (Fig. 3) and a weak crenulation lineation. The layering is of a discontinuous nature.

The average grain size of muscovite is approximately 500 μm. In thin section, the muscovite grains display a strong preferred shape orientation which defines the macroscopically visible schistosity. Moreover, muscovite forms elongated grains with the long axes parallel to the crenulation lineation, as can be observed in thin sections parallel to the schistosity. This lineation is interpreted as a stretching lineation due to the perpendicular orientation of the quartz *c*-axis girdle. A number of C′-type shear bands cut across the schistosity at an angle of 30°–40° (Fig. 3). All mica grains display continuous lattice bending, observed in sections perpendicular to the schistosity. In sections parallel to the schistosity, frequent subgrain pattern formations can be observed which indicate the activity of dislocation glide and climb.

The quartz microstructure is characterized by two grain size populations. The first population has an average grain size of approximately 300 μm and a strong shape-preferred orientation with aspect ratios ranging from 3:1 to 5:1. It occupies distinct areas far away from the shear bands. All these quartz grains display lattice bending ranging from continuous to abrupt (deformation bands). Some grains display an incipient polygonisation, in other grains deformation lamellae are observed. Grain boundaries between quartz grains are commonly interlobate. The second population of equant grains with an average grain size of approximately 30 μm is observed inside, and close to the shear bands, indicating grain boundary mobility related to shear band formation.

5. Results

5.1. Experimental pole figures

The pole figures are presented as normalized pole density distributions (multiples of a random distribution, m.r.d.) with the horizontal line parallel to the schistosity (S) and the mineral lineation at 90° and 270°. This means that the shear bands (C′) are oriented with a clockwise rotation of 30°–40° relative to the schistosity. Equal angular projection mode (circles on the pole sphere are represented as circles in the pole figure) is used to allow better judgement of the shape of the pole density distributions. The U-stage measurements of muscovite (001), (010) and (100) are approximated by the indicatrix axes (Fig. 1) because the angle between [001] and α and [100] and β, respectively, is $<2°$. Such a deviation is accepted, since it is very small compared with the expected bulk error level. Although EBSD measurements allow discrimination of the sign of some of the measured lattice directions, such a discrimination was not performed to allow comparison of pole figures obtained with different methods.

The general outline of the muscovite texture is characterized by a unique maximum of the (001) normal (Fig. 4). The maximum intensity is very high in the EBSD and U-stage pole figures (22.5 and 29.1 [m.r.d.], respectively), much higher than in the X-ray experiment (5.3 [m.r.d.]). The optically determined (010) and (100) poles cover the whole 360° sector in the foliation plane, however, the intensity distributions are not uniform. Distinct maxima indicate preferred orientation of these lattice directions in addition to their arrangement in the foliation plane. This holds true for the EBSD derived pole figures as well, even for the (025) and (−114) intensity distributions, although the submaxima are less pronounced. These two reflections are accessible without overlapping in the X-ray and neutron experiment. In contrast to the 'single grain' methods, neither (025) nor (−114) show such distinct submaxima, which also holds true for the other neutron pole figures presented in Fig. 4. Furthermore it is observed that the 'single grain' measurements are much smoother compared with the 'statistical' diffraction measurements, and the neutron pole figures are smoother compared with the X-ray pole figures.

The general outline of the EBSD and U-stage derived quartz (001) pole figure can be described as a rather wide maximum close the foliation pole which tends to form a girdle around the lineation. The (110) pole figure can be derived only from the EBSD orientation measurements. It is characterized by a wide maximum close to the lineation. Considering also the (101), (011) and (100) pole figures, it appears that the texture as a whole contains a rotational

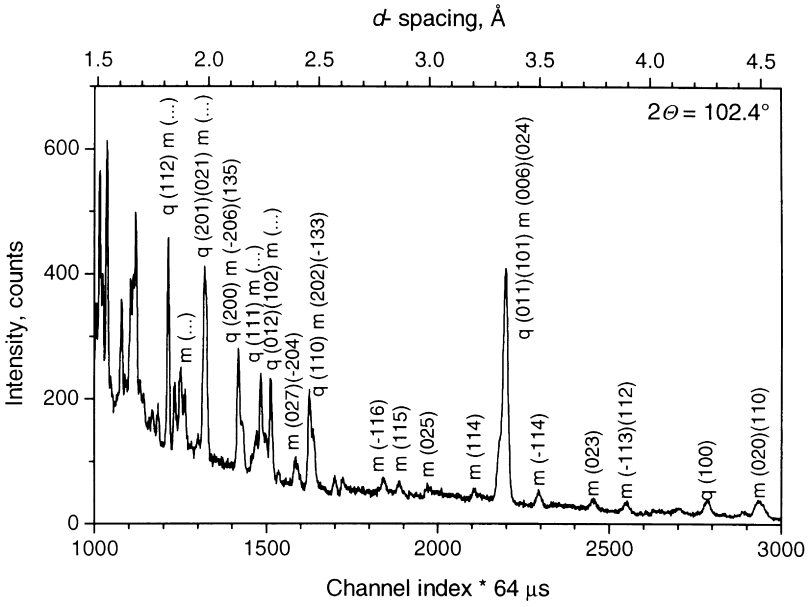

Fig. 5. Neutron time-of-flight diffraction pattern. Most quartz peaks are overlapped and must be separated during quantitative texture analysis. Moreover, all muscovite reflections are of low intensity and require long measuring times to obtain sufficient counting statistics.

component around the lineation. It is only weakly expressed in some pole figures but such a trend is important for the kinematic interpretation (see discussion below).

The 'volume' texture measurements of quartz and muscovite by means of X-ray and neutron diffraction are hampered by numerous overlapping peaks (Fig. 5). This is true for quartz in particular, where only the (100) reflection is freely accessible. The quartz (101) + (011) reflection overlaps with muscovite (006) and (024), and peak deconvolution by means of the applied X-ray measuring technique (Braun 1994) was impossible because of the very close lattice spacings of these reflections ($\Delta d \sim 0.02$ Å). In contrast, the method was applicable to the quartz (112) and (102) + (012) reflections, which could be cleared of the influence of muscovite and quartz (111). All the X-ray pole figures are different from neutron experiments. The former are more or less random, whereas the latter show clear preferred orientations. Obviously, the intensity distributions are dominated by muscovite because of the intensity arrangement on small circles with an opening angle close to the angle, which must be expected from the lattice constants of muscovite. Two reasons may explain such an effect: (1) the intensity contribution of muscovite to the experimental pole figures may be higher for neutrons as for X-rays because of a higher scattering length; (2), the preferred orientation of quartz is weak, and, as a consequence, quartz does not cause any pronounced maxima. This will be discussed below.

5.2. Axial distribution analysis

An axial distribution analysis (AVA) of quartz *c*-axes was performed on four thin sections, all of which are oriented perpendicular to the foliation and parallel to the stretching lineation. The analysis is based on four (sub)maxima of the quartz *c*-axis pole figure, which are colour-coded in Fig. 6. Without quantification of e.g. spatial distributions, geometries and grain–grain relationships using statistical methods or fractal geometry, the interpretation by a purely visual analysis is restricted. The spatial distribution of the differently oriented grains displays no significant difference between the four orientation groups. Neither the size nor the shape or distribution of grains is correlated with a preferred crystallographic orientation. The spatial distribution of grains with clearly different crystallographic orientation appears to be homogeneous. Only grains of the green and blue orientation groups form small clusters which, however, only rarely exceed more than three grains. In general, the AVA points to a rather homogeneous deformation with no strain partitioning on the thin section scale.

The grain boundary distributions (refer to Duyster, 1991 for definitions) show no significant variations (Fig. 7). The long axes of the averaged grain boundary tensors enclose an angle of 7°–14° with the lineation. The residual grains (indicated as 'gray' in Fig. 7) also fit this interval (and so does the sum of all grains, of course). It should be pointed out that the distribution of the yellow grains can be erroneous due to the small number of grains. The grain size distribution, given as grain area in micrometers squared, is rather homogeneous as well, with an average grain size ranging from 1826 to 2497 μm^2 for the four considered orientation groups, of 2009 μm^2 for the residual grains, and an overall average of 2099 μm^2.

a)

b)

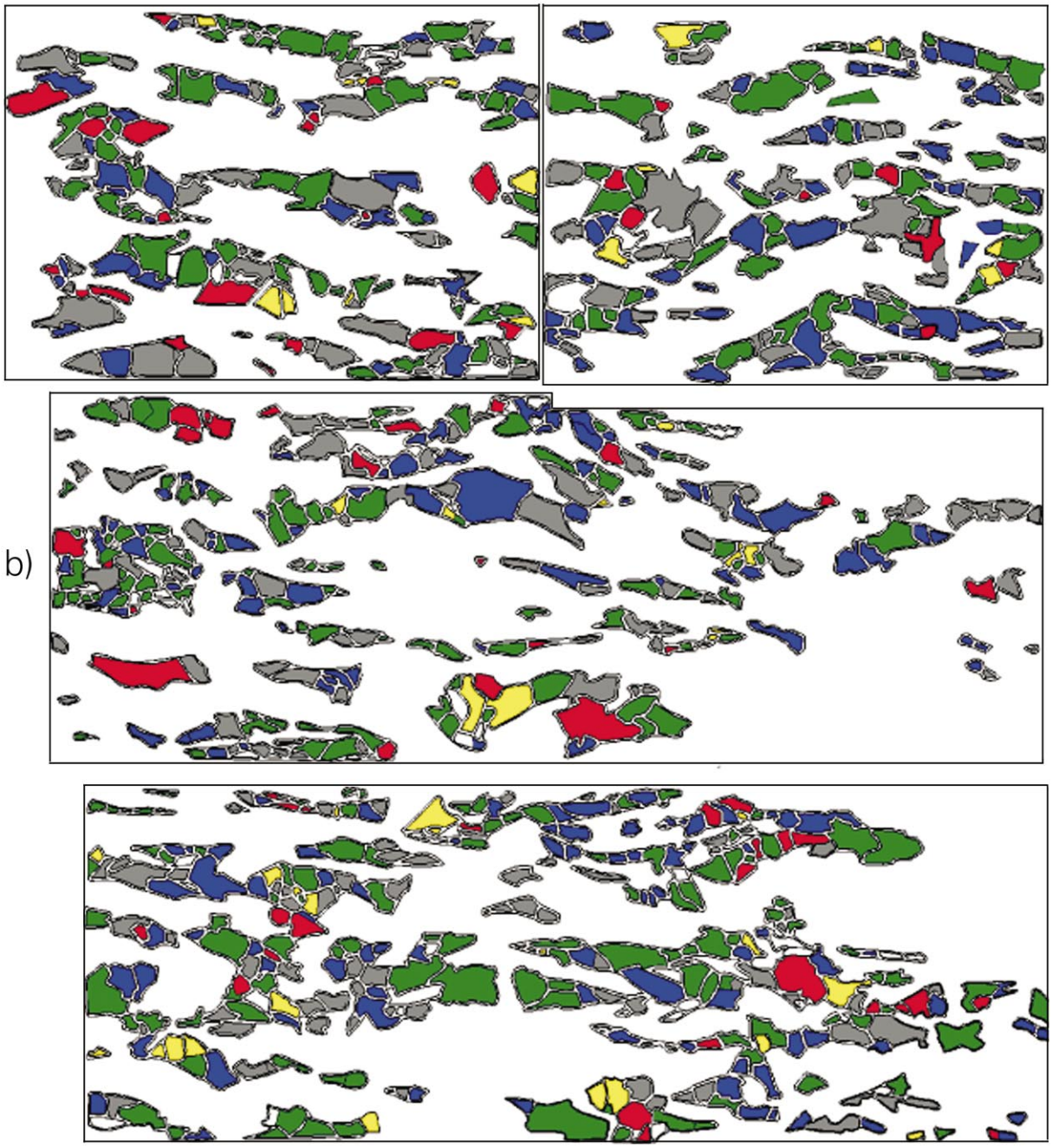

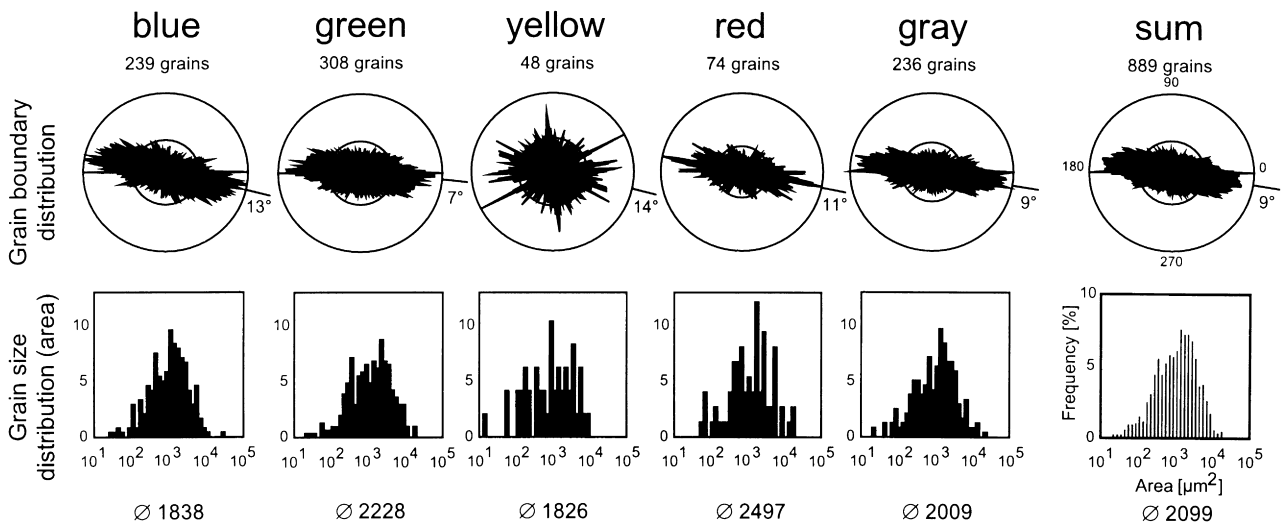

Fig. 7. Grain boundary and grain size (area) distribution of the orientation groups of Fig. 6. Gray comprises the residual orientations. The mean grain area [μm^2] is indicated at the bottom.

6. Discussion

6.1. Quantitative comparison of the pole figures

Discussion of the reliability of texture measurements with different experimental techniques should be based upon the principal properties of the applied techniques and the differences between the resulting pole figures. Texture differences can be judged more satisfactorily by means of pole figure differences ('difference pole figures') rather than by a simple visual description, since such pole figures visualize the spatial distribution of intensity differences in a quantitative way.

A quantitative comparison between volume-related pole density measurements (X-rays and neutrons) and 'single grain' measurements (EBSD and U-stage) is not easy to achieve. The resulting density distributions of the latter depend upon the method by which they are calculated (e.g. Section 3), and no relation to the grain volume is given except in the case of equant grain size. Since no mathematical relationship is reported between 'statistical' diffraction data and 'single grain' measurements, we introduced the condition that the difference between comparable pole figures should be a minimum. Initially, the 'single grain' data were rotated such that the best coincidence between the pole figures was achieved. Subsequently, the half width of a Gaussian, which fulfils this condition, was determined by an iterative procedure. The procedure could be applied to the muscovite (025), (−114), (114) and (023) reflections because they are not overlapping. An average half width of 6.3° was determined and used to calculate the pole density distributions of all EBSP and U-stage measurements with the same measuring grid as applied for the neutron texture measurements. Since the X-ray measurements are volume-related they were kept unchanged.

Comparison of the experimental pole figures that are not overlapping (see Fig. 4) shows that the EBSD and U-stage derived experimental pole figures agree quite well, even quantitively (examples in Fig. 8a). The intensity distributions in the difference pole figures are more or less uniform and display no pronounced maxima, except for muscovite (001) where rather large residuals are observed close to the position of the intensity maximum in the experimental pole figures. The residuals can be attributed to different shape of the maxima which lead to large local gradients, although the maximum intensities are approximately identical.

In contrast, comparing the X-ray and EBSD derived pole figures with the neutron pole figures as a reference (U-stage measurements are omitted since they agree well with the EBSD measurements), clear preferred orientations are commonly observed. The principle observations, illustrated by some examples, are that: (1) the 'difference pole figures' show a more or less uniform intensity distribution with no pronounced intensity maxima, e.g. the muscovite (025) pole figure measured by X-rays (Fig. 8b); (2) the intensity distributions in the 'difference pole figures' reflect a similar intensity distribution as the experimental pole figures, but in two different ways: either maxima in the 'difference pole figures' coincide with maxima in the experimental pole figures (the muscovite (−114) pole figure, Fig. 8b), or minimum regions in the 'difference pole figures' correspond to maximum regions in the experimental pole figures (the EBSD-derived 'difference pole figures', Fig. 8c).

Fig. 6. Quartz *c*-axis AVA. (a) Pole figure from Fig. 4, also given in the section perpendicular to the schistosity and parallel to the lineation and colour-coded to display the four selected orientation groups. Minimum and maximum intensity are 0.0 and 3.1 [m.r.d.], respectively. (b) Colour-coded microstructure of four thin sections perpendicular to the schistosity and parallel to the lineation.

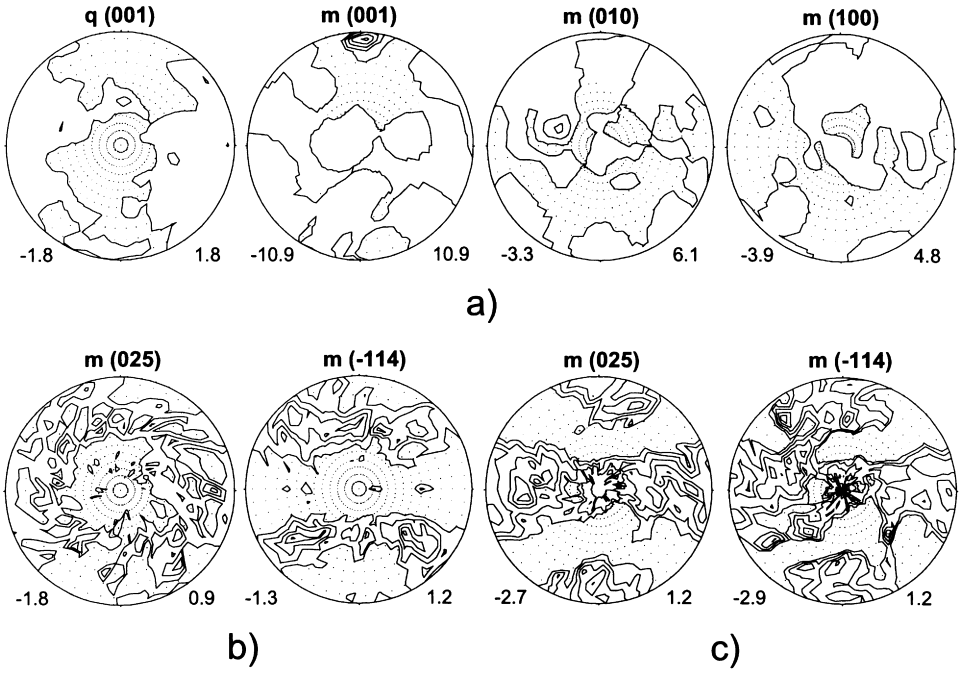

Fig. 8. Pole figure differences (a) 'EBSD–U-stage', (b) 'Neutrons–X-rays' and (c) 'Neutrons–EBSD' of some experimental pole figures. Negative regions are indicated by dots, minima and maxima are indicated at the bottom of each stereoplot.

Several factors may explain the observed phenomena. First, 'single grain' measurements are usually not volume-related in contrast to 'statistical' diffraction experiments. It is expected that the broader the grain size distribution, the larger the difference between 'single grain' and 'statistical' diffraction pole figures. Weighting based upon grain size should reduce such an influence, but this requires additional knowledge of the grain size distribution.

Second, 'single grain' and X-ray measurements are performed on the surface of the sample, whereas neutrons allow access to much larger sample volumes (Table 2). It is obvious, that the averaging of texture inhomogeneities is much more pronounced due to the much larger sample volume that is accessible. This is, however, an advantage for the calculation of physical rock properties since the property of the bulk rock has to be characterized. Furthermore, in a 'statistical' diffraction experiment with X-rays or neutrons, the grain size should correlate with the accessible sample volume to obtain sufficient grain statistics. Hence, the mean grain size can be larger in a neutron experiment.

Third, statistical errors play an important role in texture analysis and may lead to false results. The meaning of the term 'statistics' is different for 'single grain' and 'volume' texture measurements. 'Single grain' measurements consist of a number x of integers, and in this case 'statistics' refers to the magnitude of x which must be sufficiently high to be representative. The optimum performance is to measure all grains. In practice, only a small number of grains is considered, which makes the strategy of grain selection an important issue to avoid falsification of the results. 'Statistics' in an X-ray or neutron experiment refers to the level of noise, which overlaps the scattered intensity and does not originate from the lattice planes, following Bragg's law. The ratio between Bragg intensity and noise should be high enough to keep the error level low. If the peak/noise ratio is too small, the background determination near the peak of interest may be incorrect, which leads to incorrect pole figure values. A satisfactory peak/noise ratio is usually achieved by a sufficiently high exposure time, but low-intensity peaks (Fig. 5) would require measuring times of such a duration that a compromise must be found.

6.2. Implications from recalculated (ODF-derived) pole figures

From the X-ray and neutron pole figures, the muscovite

Fig. 9. Selected recalculated pole figures obtained by different methods of quantitative texture analysis. The'harmonic' and'WIMV' derived pole figures illustrate the common occurrence of artificial intensity maxima. The recalculated pole figures from two-phase component fit display the simplified texture, which is obtained by this method. The recalculated muscovite (010) pole figures display distinct maxima on a small circle around the foliation pole, which is particularly evident for the X-ray pole figures where the maxima could be reproduced by all the algorithms applied (a). In the neutron pole figures, the maxima are weaker but present (b). They are absent in the recalculated pole figure from component fit (c), which can be explained easily from the fundamental model assumptions of the method, and from the fact that the recalculated pole figure is composed of only a few ideal crystal orientations with the (001) direction close to the foliation pole.

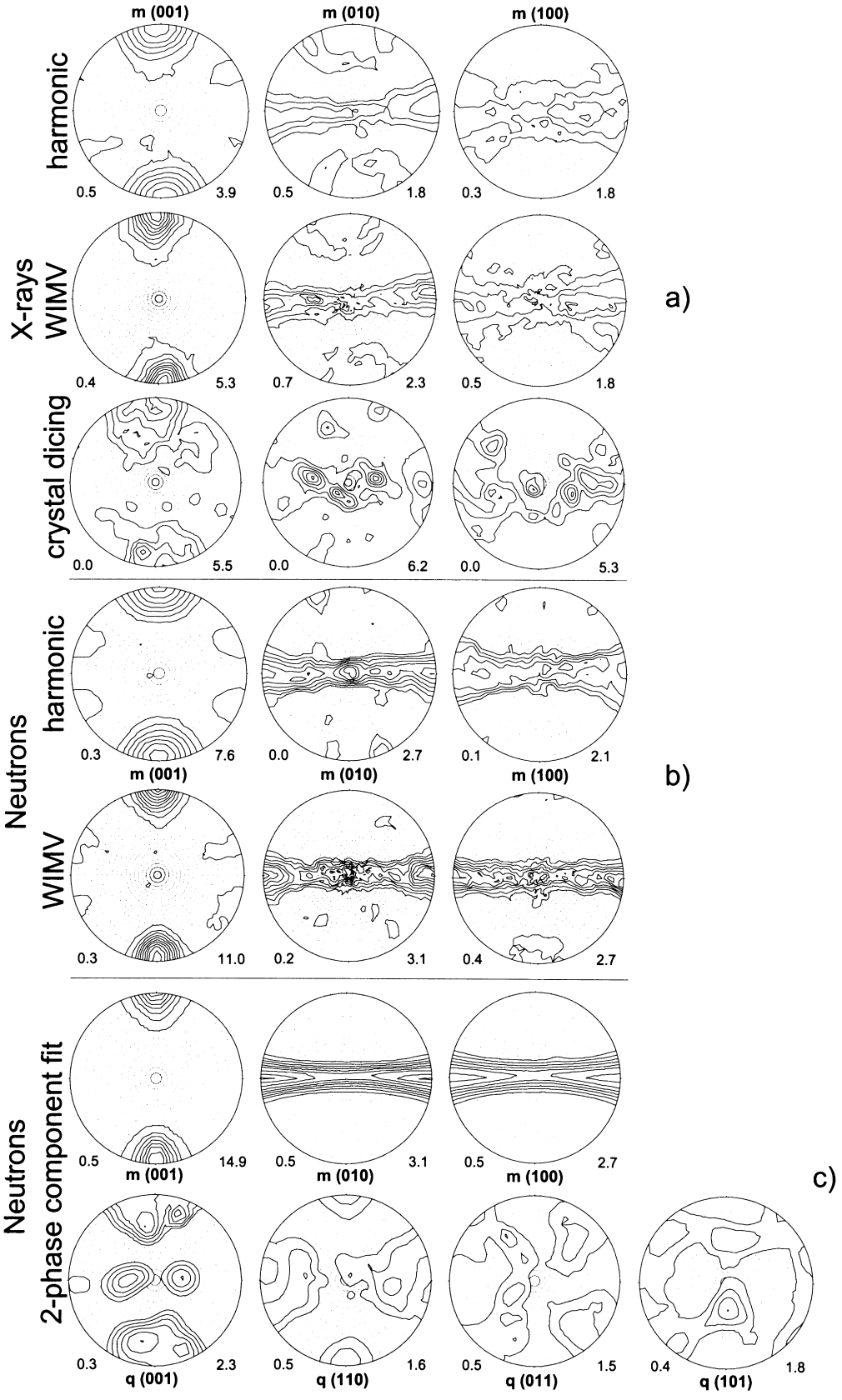
m (001)
m (010)
m (100)
harmonic
0.5 3.9
0.5 1.8
0.3 1.8
X-rays
WIMV
0.4 5.3
0.7 2.3
0.5 1.8
a)
crystal dicing
0.0 5.5
0.0 6.2
0.0 5.3
Neutrons
harmonic
0.3 7.6
0.0 2.7
0.1 2.1
m (001)
m (010)
m (100)
b)
WIMV
0.3 11.0
0.2 3.1
0.4 2.7
Neutrons
2-phase component fit
0.5 14.9
0.5 3.1
0.5 2.7
m (001)
m (010)
m (100)
c)
0.3 2.3
0.5 1.6
0.5 1.5
0.4 1.8
q (001)
q (110)
q (011)
q (101)

ODF was calculated applying the harmonic method, WIMV, 'crystal dicing' and texture component fit. These methods are widely used in the earth sciences and represent a cross-section through the basal models for quantitative texture analysis (Section 3). The goal is to evaluate especially those pole figures which are not accessible in the experiment, and to compare them with the EBSD and optical measurements.

In addition to the expected girdle in the foliation plane, the recalculated muscovite (010) pole figures display distinct maxima on a small circle around the foliation pole (Fig. 9), which is particularly evident for the X-ray pole figures where the maxima could be reproduced by all the algorithms applied (Fig. 9a). In the neutron pole figures, the maxima are weaker but present (Fig. 9b). They are absent in the recalculated pole figure from component fit (Fig. 9c), which can be explained easily from the fundamental model assumptions of the method, and from the fact that the recalculated pole figure is composed of only a few ideal crystal orientations with the (001) direction close to the foliation pole. In the (100) pole figures, uncommon maxima are only observed in the neutron-derived pole figures (Fig. 9b) With the exception of the WIMV-derived X-ray pole figure, the recalculated (001) pole figures contain weak maxima close to the lineation in addition to the expected maximum (Fig. 9a, b), even though they are used as input for the ODF calculation.

These secondary maxima, described above, are completely absent in the EBSD and U-stage derived pole figures (Fig. 4). Also, there is no relation to the orientation of the C' shear bands (Fig. 3) or any other microstructural feature. Consequently, the maxima are interpreted as artifacts. The initial assumption that the artifacts may be attributed to the method of ODF calculation is unlikely since the algorithms are quite different but lead to similar results. Any relation to the experimental technique also appears improbable. Hence, it must be concluded that the artifacts are caused by the input data. Similar observations were published recently by Schaeben et al. (1999), and the interpretation was that wrong background correction led to an erroneous ODF. If this interpretation is valid, it seems that 'statistical' texture measurements may be very sensitive to improper data correction.

The component method (Helming and Eschner, 1990; Eschner, 1993) is often applied to geological samples because it offers a minimum of restrictions. The method deals with any crystal symmetry and allows for simultaneous texture analysis of two or more phases (e.g. Siegesmund et al., 1994). This latter property enabled us to determine also the quartz texture from the neutron diffraction data, despite the occurrence of numerous overlapping reflections, even of quartz and muscovite. The recalculated pole figures (Fig. 9c) are much smoother than the pole figures obtained by other methods. This is a consequence of the simplified texture description. The recalculated muscovite pole figures are based on three axially symmetric components with the rotation axis parallel to the (001) normal. The component axes scatter slightly perpendicular to the lineation, which leads to an elliptical shape of the (001) intensity maximum. The inclination of the axes also explains the intensity maxima in the (100) and (010) pole figures, which parallels the lineation. The components intersect at this position, i.e. increased pole densities must be observed. It is obvious that such maxima have no kinematic significance because their origin is due to calculation only. The recalculated (001), (110), (011) and (101) quartz pole figures (Fig. 9c) are based on at least 16 components because of the more complicated texture compared to muscovite. Again, the pole figures appear very smooth. In principle, they show the same tendency as the EBSD-derived experimental pole figures (Fig. 4), but it is notable that the quartz (001) pole figure, which is important for the kinematic interpretation, displays the most pronounced simplification. The question arises whether the simplification of texture reproduction by means of components influences its kinematic interpretation.

6.3. Kinematic significance of the textures gained from different experimental techniques

Applying the model of Schmid and Casey (1986), the strain increment which is recorded by the quartz texture seems to be constrictional. This is indicated by the *c*-axes distribution, which may be interpreted as a small circle with a large opening angle around the lineation. This conclusion is based upon different amounts of data. In the case of U-stage measurements, only the *c*-axis pole figure may be evaluated, and some uncertainty remains whether the texture as a whole possesses a rotational component. This cannot be verified by means of optical measurements, but the EBSD technique offers such a possibility. All quartz pole figures display a tendency to form small circles around the lineation. Although this tendency is weak and the intensity distribution along the girdles is inhomogeneous, the larger number of pole figures which can be checked increases the probability that such an interpretation is valid.

In the case of diffraction measurements with X-rays or neutrons the interpretation of the quartz texture is based largely upon recalculated pole figures, since most pole figures that are important for the kinematic interpretation cannot be measured directly or only as overlapping figures. Simultaneous ODF calculation of both phases is required, since muscovite–quartz peak overlapping occurs. Recalculated quartz pole figures from two-phase component fit show the same trend as the single crystal measurements: a tendency to form a small girdle around the lineation. Also in this case, the intensity distribution along the girdles is inhomogeneous but the tendency is visible in all pole figures. The X-ray experiment did not result in pole figures with well-defined preferred orientations, hence, calculation of the ODF was not possible. This is attributed, partly to the small sample volume that is accessible during measurement,

resulting in bad counting statistics, and partly to the rather weak preferred orientation of quartz.

The nearly axially symmetric (001) pole figure of muscovite leads to the assumption that flattening strain (extensional flow) was the predominant deformation mode. Such a conclusion may be derived from (001) pole figures obtained by any experimental technique. Accordingly, all other lattice directions are arranged on circles around the (001) intensity maximum. However, the different experimental methods led to different intensity distributions. The optical and EBSD-derived pole figures show distinct submaxima on the girdles at an angle of about 45° to the lineation. It is remarkable that the submaxima have almost identical spatial orientations (Fig. 4) and cannot, therefore, be artifacts. However, the 'volume' texture measurements, especially the neutron measurements, do not show such submaxima. It appears that texture inhomogeneities were recorded by the 'single grain' measurements, and the averaging on several cubic centimeters by means of neutron diffraction is sufficient in this case to determine the bulk texture.

7. Conclusions

All commonly applied techniques of texture determination possess specific characteristics, which are related to their fundamental physical principle. This leads to some well-known restrictions such as: (1) the complete orientation of uniaxial minerals cannot be determined by optical methods; (2) the accessible sample volume in the X-ray experiment may be too small in relation to the grain size; and (3) peak overlapping limits the possibilities of X-ray and neutron diffraction. Of course, there are also well known advantages such as: (1) access to the grain location applying 'single grain' methods; and (2) integration over large sample volumes using neutrons.

Choice of the method of analysis should be based upon the scientific goals. An optical quartz *c*-axis pole figure may be sufficient to determine the shear sense in a fine-grained quartzite. Phyllosilicate (001) pole figures contain information about the small-scale foliations of rock (cleavages, shear bands), and they may be determined easily on a U-stage or with X-rays. The modelling of physical anisotropies of rocks from the mineral textures aim to characterize the bulk rock, hence, it is advantageous to use neutrons since a better averaging of texture inhomogeneities can be achieved.

Unfortunately, also external factors play a role in the decision of which method should be applied for a texture determination. Optical equipment is cheap, usually available, and the effort for sample preparation is minor since the measurements are performed on standard thin sections. Therefore, optical equipment is used commonly, although about one working day is required to determine, e.g., a quartz *c*-axis distribution. Access to X-ray equipment is quite easy as well, but the purchase of such equipment is more expensive. Backreflection texture goniometry requires polished surfaces only, i.e. the effort for sample preparation is moderate. Scanning electron microscopes are numerous but EBSD equipment is not, although the number of facilities increases. Much effort is required to prepare a highly polished acquisition surface. Neutron diffraction texture measurements are the most expensive, as they usually require travelling, and access to neutron facilities is limited due to restricted measuring time. On the other hand, sample preparation is easy since also irregular sample shapes are suitable for the neutron experiment. Common to all diffraction techniques is the amount of time to determine the texture completely, which is in the order of 24 h. Hence, the choice of an experimental technique is often a compromise between scientific requirements and economical constraints.

Hopefully, this study may help to decide whether the 'method of best choice' can be replaced by an alternative method. It is obvious that the general features of the mineral textures can be reproduced by any method, but differences in the details are crucial. This refers especially to the submaxima in the U-stage and EBSD-derived muscovite (010) and (100) pole figures. Obviously the submaxima represent local preferred orientations, which deviate from the global texture. Considering also the different degree of preferred orientation of the (001) pole figures gained with the different techniques, large discrepancies must be expected for any modeled anisotropic physical property of bulk rocks. Hence, we cannot recommend 'single grain' measurements for the modelling of rock physical anisotropies. A better approximation of the global texture may be achieved by X-rays, although it is obvious that counting statistics is close to the acceptable level. Since counting statistics largely depends upon the grain size and volume fraction of the mineral of study, the grain size of the muscovite-bearing quartzite, i.e. 300–500 μm, together with a volume fraction of about 50% seems to represent the limit for X-ray pole figure measurements. This is in agreement with our experience from numerous texture measurements with X-rays. On the other hand, information about local textures is difficult to achieve from 'volume' texture measurements. Although very small sample volumes may be examined using suitable slit systems, applications are restricted to sufficiently fine-grained materials because of the statistical nature of 'volume' texture measurements. Access to single grains is impossible. It may be achieved by 'single grain' methods, which therefore are the better choice if local textures, grain–grain relationships etc. are to be investigated.

The commonly applied methods for quantitative texture analysis led to similar texture reproduction, even in detail, except for the component method which generates a simplified ODF. In the case of the muscovite texture, simplification seems to be justified because the diffraction measurements contain no indication for any reorientation

mechanism in addition to (001) slip. The quartz texture is difficult to evaluate, since there is no reference ODF. The rotational feature of the texture may be reproduced also by texture components, but we cannot find an equivalent for the prominent *c*-axis maxima in the foliation plane. The conclusion is that a simplified ODF should be treated carefully. Especially in the case of weak textures, such as in the studied sample, a much larger number of texture components as we could find may be required to describe the main textural features. The observation of artifacts in the recalculated muscovite pole figures, which are clearly caused by the input data and not by the applied algorithm, indicate that the best possible correction of the experimental data should be achieved to avoid the risk of misinterpretations.

Acknowledgements

The suggestions of two unknown referees, which helped to improve the manuscript, are gratefully acknowledged. K.U. thanks the German Ministry for Education and Research for support through grant DUBG02 and S.S. the German Science Foundation for a Heisenberg Fellowship (Si 438/10).

References

Adam, J.F., 1989. Methoden und Algorithmen zur Verwaltung und Analyse axialer 3D-Richtungsdaten und ihrer Belegungsdichten. Göttinger Arbeiten zur Geologie und Paläontologie 49, 1–100.

Azaroff, L.V., 1968. Elements of X-ray Crystallography. McGraw-Hill, New York.

Bacon, G.E., 1975. Neutron diffraction. Clarendon Press, Oxford.

Benn, K., Mainprice, D., 1989. An interactive program for determination of plagioclase crystal axes orientations from U-stage measurements: an aid for petrofabric studies. Computers and Geosciences 12, 1127–1142.

Braun, G., 1969. Computer calculated counting nets for petrofabric and structural analysis. Neues Jahrbuch Mineralogischer Monatshefte 1969, pp. 469–476.

Braun, G., 1994. A statistical geometric method for quantitative texture analysis. In: Bunge, H.-J., Siegesmund, S., Skrotzki, W., Weber, K. (Eds.), Textures of Geological Materials, Deutsche Gesellschaft für Materialkunde, pp. 61–82 Special Publication.

Brokmeier, H.G., 1994. Application of neutron diffraction to measure preferred orientations of geological materials. In: Bunge, H.-J., Siegesmund, S., Skrotzki, W., Weber, K. (Eds.), Textures of Geological Materials, Deutsche Gesellschaft für Materialkunde, pp. 327–344 Special Publication.

Bunge, H.J., 1982. Texture Analysis in Material Science. Butterworth, London.

Burri, C., Parker, R.L., Wenk, E., 1967. Die Optische Orientierung der Plagioklase. Birkhäuser, Basel.

Chernock, W.P., Beck, P.A., 1952. Analysis of certain errors in the X-ray reflection method for the quantitative determination of preferred orientations. Journal of Applied Physics 23, 341–345.

Cumbest, R.J., 1990. Amphax: A Fortran program for calculation of the lower hemisphere stereographic projections of the crystallographic axes of clinoamphibole from universal stage measurements. Computers and Geosciences 16, 371–377.

Dahms, M., Bunge, H.-J., 1988. ODF calculation by series expansion from incompletely measured pole figures using the positivity condition—Part II. All crystal symmetries. Textures and Microstructures 8/9, 97–114.

Dahms, M., Bunge, H.-J., 1989. The iterative series-expansion method for quantitative texture analysis. I. General outline. Journal of Applied Crystallography 22, 439–447.

Decker, B.F., Asp, E.T., Harker, D., 1948. Preferred orientation determination using a Geiger counter X-ray diffraction goniometer. Journal of Applied Physics 19, 388–392.

Duyster, J., 1991. Strukturgeologische Untersuchungen im Moldanubikum (Waldviertel, Österreich) und methodische Untersuchungen zur bildanalytischen Gefügequantifizierung von Gneisen. Ph.D. thesis, Universität Göttingen.

Erskine, B.G., Heidelbach, F., Wenk, H.-R., 1993. Lattice preferred orientation and microstructures of deformed Cordilleran marbles: correlation of shear indicators and determination of strain path. Journal of Structural Geology 15, 1189–1205.

Eschner, T., 1993. Texture analysis by means of model functions. Textures and Microstructures 21, 139–146.

Helming, K., Eschner, T., 1990. A new approach to texture analysis of multiphase materials using a texture component model. Crystalline Research Technology 25, K203–K208.

Hjelen, J., Nes, E., 1990. Spatial resolution measurements of electron backscatter diffraction patterns (EBSPs) in the Scanning Electron Microscope. Proc. of the XII Int. Cong. for Electron Microscopy, San Fransico Press Inc, San Francisco, pp. 404–405.

Hjelen, J., Orsund, R., Hoel, E., Runde, P., Furu, T., Nes, E., 1993. EBSP, Progress in technique and application. Textures and Microstructures 20, 29–40.

Joy, D.C., Newbury, D.E., Davidson, D.L., 1982. Electron channeling patterns in the scanning electron microscope. Journal of Applied Physics 53, R81–R122.

Kruhl, J.H., 1987. Computer-assisted determination and presentation of crystallographic orientations of plagioclase on the basis of universal-stage measurements. Neues Jahrbuch Mineralogischer Abhandlungen 157, 185–206.

Law, R.D., 1990. Crystallographic fabric: a selective review of their application to research in structural geology. In: Knipe, R.J., Rutter, E.H. (Eds.), Deformation Mechanisms, Rheology and Tectonics. Geological Society, Special Publication 54, pp. 335–352.

Leiss, B., 1996. Strukturbezogene Textur- und Korngefügeuntersuchungen duktil deformierter Dolomitgesteine am Südwestrand des Damara Orogens (Namibia)-Mechansimen der Texturbildung und ihre kinematische Bedeutung. Geotektonische Forschungen, 84, pp. 130.

Leiss, B., Siegesmund, S., Weber, K., Olesen, N.Ø., 1994. Localized texture components of a naturally deformed dolomite—a contribution to the analysis of texture-forming processes. In: Bunge, H.-J., Siegesmund, S., Skrotzki, W., Weber, K. (Eds.), Textures of Geological Materials. Deutsche Gesellschaft für Materialkunde, pp. 261–275 Special Publication.

Lloyd, G.E., 1985. Review of instrumentation, techniques and applications of SEM in mineralogy. In: White, J.C. (Ed.), Short Course in Application of Electron Microscopy in the Earth Sciences. Mineralogical Association of Canada, pp. 151–188 11.

Matthies, S., Vinel, G.W., 1982. On the reproduction of the orientation distribution function of texturized samples from reduced pole figures using the conception of a conditional ghost correction. Physical Status Solidi(b) 112, K111–K120.

O'Brien, D.K., Wenk, H.-R., Ratschbacher, L., You, Z., 1987. Preferred orientation of phyllosilicates in phyllonites and ultramylonites. Journal of Structural Geology 9, 719–730.

Oertel, G., 1985. Phyllosilicate textures in slates. In: Wenk, H.-R. (Ed.), Preferred Orientation in Deformed Metals and Rocks: An Introduction to Modern Texture Analysis. Academic Press, Orlando, pp. 431–440.

Olesen, N.Ø., Schmidt, N.-H., 1990. The SEM/ECP technique applied on twinned quartz crystals. In: Knipe, R.J., Rutter, E.H. (Eds.), Deformation Mechanisms, Rheology and Tectonics, Geological Society, Special Publication 54, pp. 369–373.

Ortiz, M., Hermida, J.D., 1981. A method for obtaining the complete pole figure with a single sample using the SCHULZ technique. Textures of Crystalline Solids 4, 159–169.

Panozzo-Heilbronner, R., Pauli, C., 1993. Integrated spatial and orientation analysis of quartz *c*-axes by computer-aided microscopy. Journal of Structural Geology 15, 369–382.

Price, G.P., 1973. The photometric method in microstructural analysis. American Journal of Science 273, 523–537.

Rabbel, W., Siegesmund, S., Weiss, T., Pohl, M., Bohlen, T., 1998. Shear wave anisotropy of laminated lower crust beneath Urach (SW Germany): a comparison with xenoliths and with exposed lower crustal sections. Tectonophysics 298, 337–356.

Raith, M., Hörmann, P.K., Abraham, K., 1977. Petrology and metamorphic evolution of the Penninic ophiolites in the western Tauern Window (Austria). Schweizerische Mineralogisch–Petrologische Mitteilungen 57, 187–232.

Reinhard, M., 1931. Universal-Drehtischmethoden. Basel.

Sander, B., 1934. Fortschritte der Gefügekunde der Gesteine, Anwendungen, Ergebnisse, Kritik. Fortschritte der Mineralogie und Petrographie 18, 111–170.

Schaeben, H., Siemes, H., 1996. Determination and interpretation of preferred orientation with texture goniometry: An application of indicators to maximum entropy pole- to orientation density inversion. Mathematical Geology 28, 169–201.

Schaeben, H., Vadon, A., Wenk, H.-R., 1985. Vector method. In: Wenk, H.-R. (Ed.), Preferred Orientation in Deformed Metals and Rocks: An Introduction to Modern Texture Analysis. Academic Press, Orlando, pp. 123–138.

Schaeben, H., Siemes, H., Fundenberger, J.-J., 1999. False patterns of preferred orientation by erroneous background-correction. In: Szpunar, J.A. (Ed.), Proceedings of the 12th International Conference on Textures of Materials (ICOTOM12). NRC Research Press, pp. 153–155.

Schäfer, W., Jansen, E., Skowronek, R., Will, G., Kockelmann, W., Schmidt, W., Tietze-Jaensch, H., 1995. Setup and use of the ROTAX instrument at ISIS as angle-dispersive neutron powder and texture diffractometer. Nuclear Instruments and Methods in Physics Research A 364, 179–185.

Schmid, S.M., Casey, M., 1986. Complete fabric analysis of some commonly observed quartz *c*-axes patterns. Geophysical Monographs 36, 263–288.

Schmidt, N.-H., Olesen, N.Ø., 1989. Computer-aided determination of crystal-lattice orientation from electron-channeling patterns in the SEM. Canadian Mineralogists 27, 15–22.

Schulz, L.G., 1949. A direct method of determining preferred orientation of a flat reflection sample using a Geiger counter X-ray spectrometer. Journal of Applied Physics 20, 1030–1033.

Siegesmund, S., 1996. The significance of rock fabrics for the geological interpretation of geophysical anisotropies. Geotektonische Forschungen 85, 1–123.

Siegesmund, S., Helming, K., Kruse, R., 1994. Complete texture analysis of a deformed amphibolite: comparison between neutron diffraction and U-stage data. Journal of Structural Geology 16, 131–142.

Siegesmund, S., Ullemeyer, K., Weiss, T., Tschegg, E.K., 2000. Physical weathering of marbles caused by anisotropic thermal expansion. International Journal of Earth Sciences 89, 170–182.

Skrotzki, W., 1994. Mechanisms of texture development in rocks. In: Bunge, H.-J., Siegesmund, S., Skrotzki, W., Weber, K. (Eds.), Textures of Geological Materials. Deutsche Gesellschaft für Materialkunde, pp. 167–186 Special Publication.

Tröger, W.E., 1971. Optische Bestimmung der gesteinsbildenden Minerale, Teil 1. Schweizerbart, Stuttgart, pp. 1–188.

Ullemeyer, K., Spalthoff, P., Heinitz, J., Isakov, N.N., Nikitin, A.N., Weber, K., 1998. The Skat texture diffractometer at the pulsed reactor IBR-2 at Dubna: experimental layout and first measurements. Nuclear Instruments and Methods in Physics Research A 412, 80–88.

Van der Wal, D., Vissers, R.L.M., 1996. Structural petrology of the ronda peridotite, SW Spain: deformation history. Journal of Petrology 37/1, 23–43.

Von Gehlen, K., 1960. Die röntgenographische und optische Gefügeanalyse von Erzen, insbesondere mit dem Zählrohrgoniometer. Beiträge zur Mineralogie und Petrographie 7, 340–388.

Walther, K., Heinitz, J., Ullemeyer, K., Betzl, M., Wenk, H.-R., 1995. Time-of-flight texture analysis of limestone standard: Dubna results. Journal of Applied Crystallography 28, 503–507.

Wedel, A., Skrotzki, W., Weber, K., 1992. Microstructure and texture in peridotite xenoliths from the Hessian depression. Geotektonische Forschungen 78, 89–125.

Weiss, T., Siegesmund, S., Bohlen, T., 1999. Seismic, structural and petrological models of the southern subcrustal lithosphere in Southern Germany: a quantitative revaluation. Pure and Applied Geophysics 156, 53–81.

Wenk, H.-R., 1985. Measurement of pole figures. In: Wenk, H.-R. (Ed.), Preferred Orientation in Deformed Metals and Rocks: An Introduction to Modern Texture Analysis. Academic Press, Orlando, pp. 11–48.

Wenk, H.-R., Bunge, H.-J., Jansen, E., Pannetier, J., 1986. Preferred orientation of plagioclase-neutron diffraction and U-stage data. Tectonophysics 126, 271–284.